Magnetically Responsive Microbubbles as Delivery Vehicles for Targeted Sonodynamic and Antimetabolite Therapy of Pancreatic Cancer

Yingjie Sheng[#1], Estelle Beguin[#2], Heather Nesbitt[#1], Sukanta Kamila[1], Joshua Owen[2], Lester C. Barnsley[2], Bridgeen Callan[1], Christopher O'Kane[3], Nikolitsa Nomikou[4], Rifat Hamoudi[4,8], Mark A. Taylor[5], Mark Love[6], Paul Kelly[7], Declan O'Rourke[7], Eleanor Stride*[2], Anthony P. McHale*[1] and John F. Callan*[1].

1. Biomedical Sciences Research Institute, University of Ulster, Coleraine, Northern Ireland, U.K. BT52 1SA. 2. Institute of Biomedical Engineering, University of Oxford, UK, OX3 7DQ. 3. Department of Biomedical and Forensic Science, Anglia Ruskin University, Cambridge, UK, CB1 1PT. 4. Division of Surgery & Interventional Science, Faculty of Medical Sciences, University College London, UK; 5. Department of HPB Surgery, Mater Hospital, Belfast, Northern Ireland, U.K. BT14 6AB. 6. Imaging Centre, The Royal Victoria Hospital, Grosvenor Road, Belfast, Northern Ireland, U.K. BT12 6BA; 7. Department of Pathology, The Royal Victoria Hospital, Grosvenor Road, Belfast, Northern Ireland, U.K. BT12 6BA. 8. Sharjah Institute for Medical Research, College of Medicine, University of Sharjah, Sharjah, UAE.

[#] *Joint first authors. * To whom correspondence should be addressed.*

Abstract: Magnetically responsive microbubbles (MagMBs), consisting of an oxygen gas core and a phospholipid coating functionalised with Rose Bengal (RB) and/or 5-fluorouracil (5-FU), were assessed as a delivery vehicle for the targeted treatment of pancreatic cancer using combined antimetabolite and sonodynamic therapy (SDT). MagMBs delivering the combined 5-FU/SDT treatment produced a reduction in cell viability of over 50% when tested against a panel of four pancreatic cancer cell lines *in vitro*. Intravenous administration of the MagMBs to mice bearing orthotopic human xenograft BxPC-3 tumours yielded a 48.3% reduction in tumour volume relative to an untreated control group ($p<0.05$) when the tumour was exposed to both external magnetic and ultrasound fields during administration of the MagMBs. In contrast, application of an external ultrasound field alone resulted in a 27% reduction in tumour volume. In addition, activated caspase and BAX protein levels were both observed to be significantly elevated in tumours harvested from animals treated with the MagMBs in the presence of magnetic and ultrasonic fields when compared to expression of those proteins in tumours from

either the control or ultrasound field only groups ($p<0.05$). These results suggest MagMBs have considerable potential as a platform to enable the targeted delivery of combined sonodynamic / antimetabolite therapy in pancreatic cancer.

Key words: Microbubbles, magnetic targeting, drug delivery, hypoxia, 5-fluoruracil, Rose Bengal, sonodynamic therapy, antimetabolite therapy, pancreatic cancer.

1.0 Introduction: Pancreatic cancer has the lowest survival rate among the 21 most common forms of cancer with only 3% of patients surviving five years after their initial diagnosis [1]. Whilst many other forms of cancer have seen survival rates increase significantly over the past four decades, the survival rate for pancreatic cancer has remained unchanged. Late presentation of patients due to the vague symptoms associated with the disease means only ~ 20% are eligible for potentially curative resection at the time of initial diagnosis [2]. Of the remaining ~ 80% of patients, ~50% present with metastatic disease and ~30% with locally advanced or borderline resectable pancreatic cancer (LAPC or BRPC) [3]. While earlier diagnosis and better awareness are key components of any future strategy to improve survival rates, there is also an urgent need for improved therapies. Several studies have investigated the potential of neo-adjuvant chemo- and / or radio-therapy to downstage tumours and increase the number of patients eligible for resection [3,4,5]. Unfortunately, such treatments are often associated with significant off-target effects due to the non-specific nature of the chemotherapy regimen. Therefore, the development of targeted treatments that reduce side-effects related to systemic chemotherapy have enormous potential as neo-adjuvant and palliative pancreatic cancer treatments by reducing tumour burden to either enable surgery or to provide symptom relief.

In a previous study, we demonstrated the utility of ultrasound responsive microbubbles (MBs) for delivery of drug payloads and encapsulated oxygen gas to pancreatic tumours [6]. MBs are lipid or polymer stabilised gas filled particles approved for use as contrast agents in diagnostic ultrasound [7]. At low ultrasound pressures, MBs oscillate in a relatively symmetric manner resulting in acoustic backscatter that enhances the quality of the diagnostic image [8]. Exposure of cells to low intensity ultrasound can also facilitate a phenomenon known as sonoporation which causes a transient 'poration' of cellular plasma membranes and the phenomenon is enhanced in the presence of exogenously-added MBs. Such an approach has been exploited to enhance the efficacy of gemcitabine therapy in pancreatic cancer patients [9-10]. In contrast, at higher acoustic pressures, collapse of the MB leads to rupture and release of the shell fragments at the target site [11]. This feature has been exploited by several groups investigating the potential of MBs as targeted delivery vehicles [12,13]. In our previous work, we attached the antimetabolite drug 5-fluouracil (5-FU) and the sonosensitiser Rose Bengal (RB) to the shell of oxygen-loaded lipid stabilised MBs for the combined antimetabolite and sonodynamic therapy (SDT) treatment of pancreatic cancer [6]. Significant reductions in the viability of three pancreatic cancer cell lines (BxPC3, MiaPaCa-2 and Panc-01) and inhibition of the growth of ectopic pancreatic BxPC-3 tumours were observed for the combined treatment when compared to either treatment alone. Antimetabolite therapy is an established treatment protocol for pancreatic cancer with 5-FU and gemcitabine among the most commonly used antimetabolite drugs [14]. In contrast, SDT is an emerging anti-cancer treatment that involves the activation of an otherwise inactive sensitiser drug using low-intensity ultrasound [15]. The combination of sensitiser and ultrasound, in the presence of molecular oxygen, generates cytotoxic levels of reactive oxygen species (ROS) causing cell death via oxidative stress [16]. As oxygen is a key substrate for the generation of ROS in SDT, and since pancreatic adenocarcinoma is characterised as extremely hypoxic, providing oxygen during SDT can improve the ROS yield and enhance the therapeutic outcome [17]. While our oxygen carrying

MBs have shown great promise as a platform for targeted oxygen delivery and enhanced 5-FU / SDT treatment of pancreatic cancer, there remains a need to demonstrate the effectiveness of this method in an orthotopic tumour model following intravenous injection of the MB suspension. To this end, we have reasoned that an additional layer of targeting may be required to help retain MBs in the tumour vasculature after injection and enhance the quantity of MBs destroyed at the target site by ultrasound exposure. The incorporation of magnetic nanoparticles within the MB shell is one approach that has been explored to improve the targeting capability of MBs. [18]. Previous work in our laboratory has demonstrated that externally applied magnetic fields may be used to enhance the retention of magnetically-responsive microbubbles at a target site in an *ex vivo* model under physiologically-relevant flow rates [19]. In this manuscript, we assess the ability of oxygen loaded magnetic MBs with 5-FU and Rose Bengal attached to their surface, as a targeted treatment for orthotopic human pancreatic BxPC-3 tumours in SCID mice. The benefit afforded by incorporating magnetic targeting into our delivery platform is demonstrated by studies in a flow-phantom and by therapeutic efficacy studies *in vivo*.

2.0 Materials and Methods

2.1 Reagents and Equipment: 1,2-dibehenoyl-sn-glycero-3-phosphocholine (DBPC) and 1,2-distearoyl-sn-glycero-3-phosphoethanolamine-N-[methoxy(polyethylene glycol) -2000] (DSPE-PEG(2000)) and DSPE-PEG(2000)-biotin were purchased from Avanti Polar Lipids (Alabaster, Alabama, USA). Oxygen gas was purchased from BOC Industrial Gases UK and perfluorobutane (PFB) was purchased from Apollo Scientific Ltd. Phosphate Buffered Saline (PBS) was purchased from Gibco, Life Technologies, UK. Glycerol and propylene glycol (1kg, hydrolysed) were purchased from Sigma Aldrich (UK). Superparamagnetic iron oxide nanoparticles (SPION): fluidMAG-Lipid (50 nm hydrodynamic diameter) were purchased from Chemicell (Berlin, Germany). The use of lipid conjugated SPION in this study was preferred over the use of previously reported isoparaffin stabilised SPION as the addition of lipids to lipid-

shelled microbubbles is likely to be less disruptive to the acoustic response of the system compared to the addition of isoparaffin [19]. These microbubbles have been extensively characterised and successfully used in previous *in vivo* experiments [20]. The method for magnetic microbubble fabrication used in this study has then been adapted for the use of lipid conjugated SPION: fluidMAG-Lipid as presented in the following section. MBs were formed using a Microson ultrasonic cell disruptor, 100 W, 22.5 kHz, from Misonix Inc. (NY, USA). Optical microscope images were obtained using a Leica DM500 optical microscope. MB concentration and size were determined using purpose- written MATLAB software (2010B, MathWorks, Natick, MA, USA). Rose Bengal sodium salt, NHS-biotin, MTT assay kit, avidin, chloroacetic acid, 4-dimethylaminopyridine (DMAP), hydroxybenzotriazole (HOBt), N,N'-dicyclohexylcarbodiimide (DCC), anhydrous dimethylformamide (DMF), and ethanol were purchased from Sigma Aldrich (UK) at the highest grade possible. Biotin, 5-Flurouracil, di(N-succinimidyl)carbonate and 2-aminoethanol were purchased from Tokyo Chemical Industry UK Ltd. Error was expressed as ± SEM (standard error of the mean) and statistical comparisons were established using ANOVA and un-paired student's t-test .

2.2 Preparation of Avidin functionalised Magnetic Microbubbles (MagPFBMBs): Avidin functionalised magnetic MBs were prepared by dissolving DBPC (4.0 mg, 4.43 µmol), DSPE-PEG(2000) (1.35 mg, 0.481 µmol) and DSPE-PEG(2000)-biotin (1.45 mg, 0.481 µmol) at a molar ratio of 82:9:9 in chloroform (274 µL). The chloroform solvent was slowly evaporated by heating the lipid solution at 40^{o}C overnight to produce a dried lipid film. The lipid film was reconstituted in 2 mL of a PBS (pH 7.4 ± 0.1) : propylene glycol : glycerol (8:1:1 v/v) mixture and the contents heated at 80^{o}C under stirring for 30 min in a water bath. FluidMAG-Lipids NPs (150 µL) were then added to the solution and the mixture was sonicated with a handheld sonicator probe for 1.5 min (100 W, 22.5 kHz, power setting 4). The headspace of the glass vial was then filled with perfluorobutane gas (PFB) and the gas / liquid interface was sonicated for 20 s (power

setting 19), producing PFB-containing magnetic MBs (MagPFBMBs). The vial was immediately sealed and placed in an ice bath for 10 min. The MagPFBMB suspension was then centrifuged (100 RCF, 5 min) to remove the excess NPs and non-incorporated MB lipids by discarding the infranatant. The microbubble concentrate was re-suspended in 2 mL of PBS (pH 7.4 ± 0.1) : propylene glycol : glycerol (8:1:1 v/v), avidin in PBS (50 µL, 10 mg/mL) was added to the suspension and the contents mixed for 10 min on a rotary shaker. The suspension was centrifuged (100 RCF, 5 min) to remove the excess avidin and the PFBMBs were again re-suspended in 2 mL of PBS (pH 7.4 ± 0.1) : propylene glycol : glycerol (8:1:1 v/v). MagPFBMBs were analysed using a Leica DM500 optical microscope to obtain the size distribution and concentration. For this, 10 µL of suspension was diluted in 190 µL of PBS and examined using a haemocytometer (Bright-Line, Hausser Scientific, Horsham, PA, USA). 30 images were obtained with a 40x objective lens and analysed with customised image analysis package in MATLAB (2010B, MathWorks, Natick, MA, USA). The iron content in the MagPFBMBs was determined by atomic absorption spectroscopy using a Varian fast sequential atomic absorption spectrometer. A calibration curve was constructed using known concentrations of Fe(III) in 0.5M HCl. Readings were taken at 248.3nm, 0.5nm slit width, 10.0mA lamp current, with the following flame settings; flame type: air/acetylene, air flow: 13.50 L/min, acetylene flow: 2.00 L/min, burner height: 13.5mm. A 300 µL sample of MagMBs was sonicated to destroy the bubbles and dissolved in 0.5M HCl. The amount of Fe(III) present in the sample was calculated by reference to the calibration curve and the total iron content determined using a magnetite (Fe_3O_4) Fe(III) : Fe(II) ratio of 2:1.

2.3 Preparation of MagO_2MB-Rose Bengal and MagO_2MB-5FU conjugates: The synthesis of biotin functionalised Rose Bengal [16] and biotin functionalised 5-FU [6] have been described by us in previous communications. Saturated solutions of biotin-RB and biotin 5-FU were prepared in a 0.5% (v/v) DMSO : PBS (pH 7.4 ± 0.1) solvent mixture. 100 µL of biotin-5FU and biotin-RB

were added to separate samples (2mL each) of MagPFBMBs and allowed to mix for 5 min on a rotary shaker. Both samples were centrifuged (100 RCF, 5 min) to remove unbound material and PFBMB conjugates were re-suspended in 1 mL of PBS solution (pH 7.4 ± 0.1). This conjugation / centrifugation process was repeated three times. The final PFBMB-RB and PFBMB-5FU conjugates were transferred to glass vials. MagO_2MB-RB and MagO_2MB-5FU conjugates were obtained by sparging the MagPFBMB-RB and MagPFBMB-5FU with pure O_2 gas for 2 min and sealing the vial via crimping. A small sample (100 µL) of both the MagO_2MB-RB and MagO_2MB-5FU conjugates was retained and the MB number again counted using a haemocytometer. The remaining sample was sonicated in an ultrasonic bath for 5 min to burst the MBs and the Rose Bengal and 5-FU concentration determined using UV-Vis (ultra violet – visible) spectroscopy and HPLC (high performance liquid chromatography) respectively [21].

2.4 Retention of MagMBs in a flow cell using an external magnetic field: MagPFBMBs without payload were used in this study to reduce wastage of biotin-5FU and biotin-RB. 1×10^7 MagPFBMBs were placed in a 1 mL syringe, connected to an ibidi µ-Slide VI flow chamber using silicone tubing (1.6 mm internal diameter) and placed in a peristaltic syringe pump. A single N52 grade NdFeB permanent magnet cube (12.7 mm) with an internal magnetization of 1.14×10^6 A/m was positioned 1 mm from the base of the flow chamber. Values for a field of 0.46 T and gradient of 83.1 T/m inside the flow chamber were calculated using a model described and experimentally verified previously [22], whereby the field was determined by breaking the magnet into a 3-dimensional lattice of evenly-distributed point moments, and summing the contributed dipole field from each moment. The MagPFBMBs were pumped through the flow chamber at a rate of 0.6 mL/min. Once the syringe was empty, the magnetic field was removed and 1 mL of PBS (pH 7.4 ± 0.1) added to the syringe to flush the flow chamber's content into a clean vial. Collected MBs were counted using the method described above. As a control, the

experiment was repeated in the absence of a magnetic field but under otherwise identical conditions. The number of MBs collected during the PBS flush was again recorded.

2.5 *In vitro* cell viability: Human primary pancreatic adenocarcinoma cell lines Mia PaCa-2 and Panc-1, were maintained in DMEM medium. The mouse primary pancreatic adenocarcinoma T110299 derived from a GEM mouse (KPC and a gift from Prof. J. Siveke, Technical University of Munich, Germany), was also maintained in DMEM medium while the human primary pancreatic adenocarcinoma cell line BxPc-3 was maintained in RPMI-1640 medium, all of which were supplemented with 10% (v/v) foetal bovine serum and grown in a humidified 5% CO_2 atmosphere at 37°C. These cells were plated into the wells of a 96-well tissue culture plate at a concentration of 5×10^3 cells per well and incubated for 24 h at 37 °C in a humidified 5% CO_2 atmosphere. The media was then removed from each well and replaced with 100 µL of treatment suspension and 100 µL of fresh mediium. This resulted in a final MB count and RB or 5-FU concentration as follows: $MagO_2$MB-RB: 10^6 MB, [RB] = 5 µM; $MagO_2$MB-5FU; 10^7 MB, [5-FU] = 100 µM and combined $MagO_2$MB-RB / $MagO_2$MB-5FU: 10^7 MB, [RB] = 5 µM, [5-FU] = 100 µM. Where required, individual wells were then placed in direct contact with the emitting surface a Sonidel SP100 sonoporator with ultrasound gel used to mediate contact. Each well was treated with ultrasound for 30 s, using a frequency of 1 MHz, an ultrasound power density of 3.0 W cm^{-2} (I_{SATP}; spatial average, temporal peak) corresponding to a peak to peak pressure of 0.8 MPa in water and 0.5 MPa inside the well as measured with a needle hydrophone (Precision Acoustics, Dorset, UK); and a duty cycle of 50% (pulse frequency = 100 Hz). The solution was then removed from the wells and fresh medium added (200 µL). Plates were incubated in a humidified 5% CO_2 atmosphere at 37 °C for 21 h and cell viability determined using an MTT assay [23]. Results were compared with those obtained using untreated cells and cells exposed to ultrasound treatment alone.

2.6 Treatment of orthotopic BxPC-3 Luc tumours in SCID mice: All animals employed in this study were treated humanely and in accordance with licenced procedures under the UK Animals (Scientific Procedures) Act 1986. BxPc-3 Luc cells were maintained in RPMI-1640 medium supplemented with 10% foetal calf serum as described above. Cells (1 x10^6) were re-suspended in 100 µL of Matrigel® and orthotopically implanted into the head of the pancreas of female Balb/c SCID (C.B-17/IcrHan®Hsd-Prkdcscid) mice. 19 days after implantation, animals were randomly distributed into 3 groups (n=4). Following induction of anaesthesia (intraperitoneal injection of Hypnorm/Hypnovel), a 100 µL mixture of PBS containing $MagO_2$MB-RB / $MagO_2$MB-5FU (MB = 1.6 x 10^8, [RB] = 350 µM and [5-FU] = 700 µM) was administered by tail vein injection to Groups 2 & 3 while Group 1 received vehicle only. For Group 2, ultrasound (frequency =1 MHz, ultrasound power density = 3.5 Wcm^{-2} I_{SATP}; spatial average temporal peak, corresponding to a free field peak to peak pressure of 0.85 MPa, duty cycle = 30% and pulse repetition frequency = 100 Hz) was directed to the tumour region (determined using prior bioluminescent imaging) via the abdomen for 3.5 min during and after injection (3.5 min total). For Group 3, in addition to ultrasound using the above parameters, a stack of permanent magnet discs (arranged to deliver the optimal magnetic force to the tumour region) [24] was directed to the tumour region (again via the abdomen) for 3.5 min during and after injection (3.5 min total), resulting in an approximate magnetic field at the tumour of 0.10 T and gradient 14.9 T m^{-1}. Treatments using the above conditions were repeated on days 20 and 21 with animals sacrificed on day 28. Tumours were then surgically excised and tumour volumes determined by direct measurement.

2.7 Determination of apoptotic marker expression in tumours post treatment: Following the determination of tumour volume a single cell suspension was prepared from the excised tumours. This involved homogenising the tumour tissue in 4 % FCS in RPMI 160 uL (30 mg/ml) collagenase type II, 50 µL (2 µg/ml) DNAse and stirring for 15 min at room temperature. A

further 160µL of collagenase II was subsequently added and the contents stirred for a further 15 min. The mixture was filtered through a 100 µm filter, centrifuged at 1700 rpm for 5 min and re-suspended in 1mL of Red Cell Lysis Buffer (RCLB) for 10 min. RCLB was neutralised by adding media containing FCS and cells were recovered by centrifuging at 1700 rpm. The pellet was washed twice with PBS, centrifuged and re-suspended in 700 µL PBS buffer. For BAX expression, 300 µL of single cell suspension in staining buffer was permeabilised using BD permeablisation buffer (BD Biosciences UK). Permeabilised cells were re-suspended in 300 µL of staining buffer containing BAX antibody (Cell Signalling Technology, D2E11) (10 µg/ml) and incubated for 30 min at room temperature. The cells were washed in ice cold PBS and the cell pellet was re-suspended in FITC secondary antibody (Abcam, ab6717-1) for 1 hour. Cells were washed three times by centrifugation at 400 RCF for 5 min in ice cold PBS, re-suspended in 650 µL of PBS buffer nd analysed by flow cytometry. For active caspase expression, the Pan Caspase NIR probe kit (Vergent Bioscience) was used according to the manufacturer's instructions. The kit utilizes the caspase family inhibitor VAD-FMK conjugated to a near IR dye (780-VAD-FMK) as a marker that irreversibly binds to activated caspases in apoptotic cells. Essentially, 300 µL of tumour single cell suspension diluted in staining buffer was centrifuged, the pellet re-suspended in 300 µL of 1XCAS-MAP NIR probe and incubated at room temperature in the dark for 1 hour. Cells were washed three times by centrifugation at 400 RCF for 5 min in ice cold PBS and re-suspended in 650 µL of staining buffer and analysed by flow cytometry. qRT-PCR was used to investigate the expression of TMBIM1 in tumours as previously described [6]. Briefly, RNA was extracted from microdissected slides using the RecoverAll Kit (Life Technologies, Paisley, UK). cDNA synthesis was carried out using the Superscript III First Strand cDNA synthesis kit (Life Technologies, Paisley, UK) using the reverse primer of each of TMBIM1 (transmembrane BAX inhibitor motif containing 1) and the two housekeeping genes;18S rRNA and b-actin. qRT-PCR was carried out using the SYBR Green kit on the CFX96 instrument (BioRad, UK). The qRT-PCR cycle was as follows: 95 C for

3 min, 95 C for 10 s, 60 C for 45 s for 40 cycles. For analysis, the geometric mean of 18S rRNA and b-actin was taken as the single housekeeping value. Statistical comparison between the groups was carried out using two-way ANOVA with Bonferroni post-hoc analysis. The primers used to investigate the TMBIM1 expression are shown in the table below.

Primer	Sequence
TMBIM1 Forward	CATCACTGCGGTGGTATCCA
TMBIM1_Reverse	GTATTGGAAGTAGAGCACAATGCTAGT
β-Actin Forward	CGTGGGCCGCCCTAGGCACCA
β-Actin Reverse	TTGGCCTTAGGGTTCAGGGGGG
18SrRNA_Forward	TGACTCAACACGGGAAACC
18SrRNA_Reverse	TCGCTCCACCAACTAAGAAC

2.8 Toxicity determination of $MagO_2MB$-5FU and $MagO_2MB$-RB conjugates: Healthy MF1 mice (8 weeks old) were randomly distributed into four groups (n=10). Group 1 received no treatment; Groups 2 & 3 received a tail vein injection (100 µL) of 5-FU (115 mM) or RB (1.03 mM) respectively and Group 4 received a tail vein injection (100 µL) containing a suspension of $MagO_2MB$-RB / $MagO_2MB$-5FU ([MB] = 2.3 x 10^8, [RB] = 570 ± 15 µM, and [5FU] = 503 ± 7 µM] on Day 1 and Day 8. Pre-treatment tail vein bleeds (0.10 mL) were collected in lithium heparinised tubes on Day 0 with the post-treatment bleeds taken in a similar manner on Day 15. Blood samples were sent to CTDS Ltd (Leeds, UK) for whole blood and plasma biochemical analysis. Urea, alanine aminotransferase (ALT), red blood cell (RBC), haemoglobin (Hb), haematocrit (HCT), mean corpuscular volume (MCV), mean corpuscular haemoglobin (MCH), mean corpuscular haemoglobin concentration (MCHC), platelet, white blood cell, neutrophil and lymphocyte levels were determined using accredited protocols. Following the day 15 bleed,

mice were then sacrificed and the liver and kidneys were surgically excised and placed in a formalin free tissue fixative solution (Sigma-Aldrich) for 24 hours. It should be noted that the liver was chosen in these studies because it has been shown that MB are removed from circulation by that organ following intravenous administration. The tissue was then placed in an automated Leica TP1020 tissue processor and passed between increasing concentrations of ethanol followed by xylene and paraffin wax 24 hours later. The wax embedded tissue samples were placed in moulds containing paraffin wax. Once the wax blocks had solidified, 5 µm sections were cut, placed on a glass slide and stained with haematoxylin and eosin (H&E) using an automated staining protocol. In some cases, additional stains (i.e. reticulin, Masson's trichrome, Perl's Prussian blue stain) were used if required. The stained sections were reviewed histologically by pathologists with expertise in liver and renal pathology. Liver architecture was initially assessed to establish if there was significant remodelling or fibrosis. The various liver compartments were subsequently examined for pathological changes. Portal tract and lobular inflammation grading was adapted from the Ishak (modified HAI) system [25]. Portal tract inflammation was graded numerically from 1 (none) to severe, affecting all portal tracts (5). Lobular inflammation was assessed at x10 magnification and graded as 1 (none) to 4 (severe, typically averaging >10 foci per x10 field). Fatty liver disease grading, referred to as steatosis/steatohepatitis, was undertaken based on parameters assessed in the NAFLD activity score [26]. In short, steatosis was graded based on a visual estimate of the percentage of liver cells affected as 1 = none or less than 5%; 2 = mild, (5- 33%); 3 = moderate (34 – 66%) and 4 = severe (greater than 67%). Kidney analysis was undertaken following a similar approach assessing the glomerular cellularity, glomerular basement membrane, tubular vacuolation, interstitial inflammation, interstitial fibrosis, vessel integrity and the collecting system. Statistical analysis was undertaken using a student's t-test where the $MagO_2$MB-RB / $MagO_2$MB-5FU group was compared directly with the 5-FU, RB and untreated groups.

3.0 Results and Discussion: Magnetic microbubbles (MagMBs) were prepared by sonication of DBPC, DSPE-PEG(2000) and DSPE-PEG(2000)-biotin lipids in the presence of PFB gas and superparamagnetic iron oxide nanoparticles (NPs). The magnetic nanoparticle formulation comprised an iron oxide core with a lipid coating to facilitate incorporation of the magnetic nanoparticles into the MB shell. The PFB containing MagMBs (MagPFBMBs) produced had an average diameter of 1 - 2 μm with a concentration of approximately 1 x 10^9 MB/mL as determined by analysis of optical microscopy images (Figure 1).

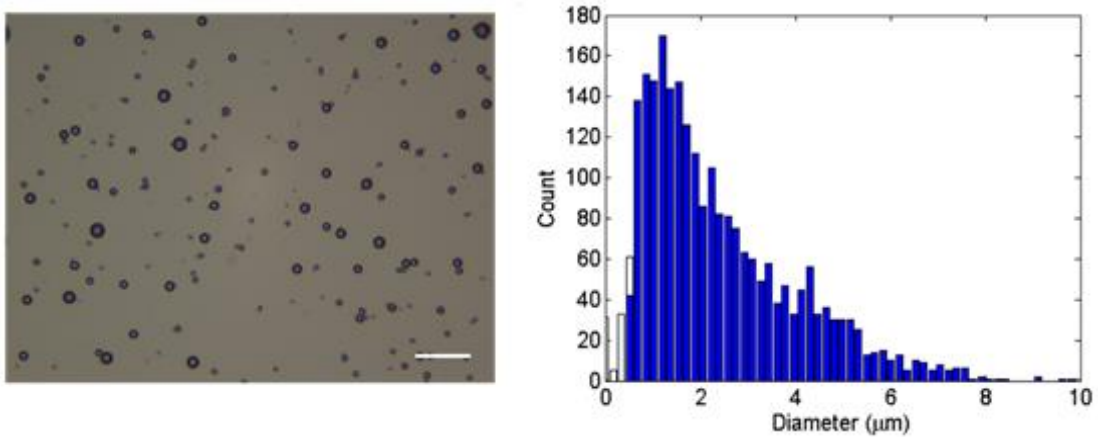

Figure 1 (a) Photomicrograph taken with a 40x objective lens of MagMBs after centrifugation (300 RCF, 5 min) and after dilution (1:20) in PBS. Scale bar is 20 μm. (b) Size distribution of MagMBs obtained from analysis of 30 optical microscope images. White boxes on the left represent microbubbles detected by the image analysis software but smaller than 450 nm, the optical resolution of the system.

The iron content of the MagPFBMBs was also determined using atomic absorption spectroscopy and revealed the MBs contained 0.286 mg/10^9 MBs total iron content. Following isolation of the MagPFBMBs by centrifugation and surface coating with avidin, biotinylated Rose Bengal and biotinylated 5-FU were added to separate batches of the MagPFBMBs to generate Rose Bengal loaded MagPFBMBs (MagPFBMB-RB) and 5-FU loaded MagPFBMBs (MagPFBMB-5FU) respectively. The PFB core gas was then exchanged with oxygen by

sparging with pure oxygen gas for 2 min generating the $MagO_2MB$-RB and $MagO_2MB$-5FU conjugates (Scheme 1).

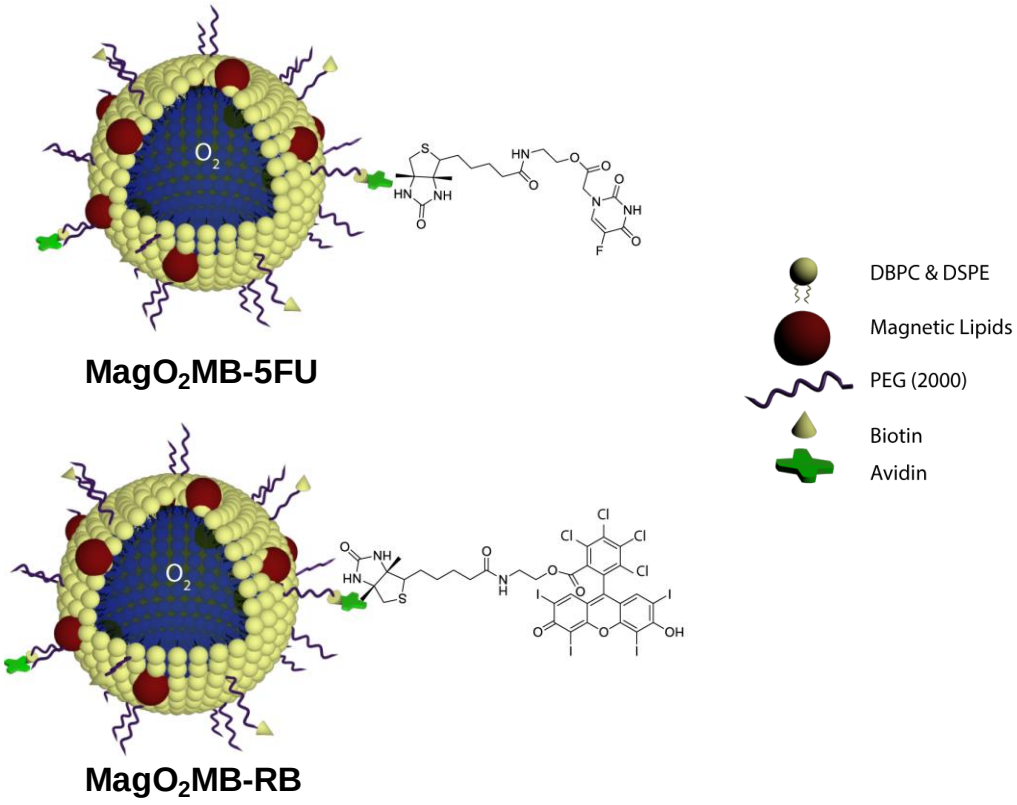

Scheme 1 Schematic representation of the $MagO_2MB$-5FU and $MagO_2MB$-RB conjugates.

To determine the magnetic response of the MB platform, suspensions of MagMBs (1 mL) were placed in a syringe and pumped through a flow chamber (0.6 mL/min) with a fixed magnet (0.46 T) positioned on the underside of the flow chamber during the course of the experiment. A control study was also performed in the absence of a fixed magnet but under otherwise identical conditions. The number of MBs retained in the flow cell at the end of each experiment were counted and the results are shown in Figure 2. A significant increase in the number of MBs ($p<0.01$) was observed when the fixed magnet was present indicating the ability of the MagMBs to be retained against flow using an external magnetic field. Blood flow rates within the human body vary considerably depending on vessel type and size with blood leaving

the aorta (2400 cm min^{-1}) at a flow rate approximately 3 orders of magnitude greater than in capillaries (1.8 cm min^{-1}) [27]. In tumours, the increased viscous and geometrical resistance presented by the vasculature can compromise its blood flow, meaning the average velocity of blood in tumour vessels can be an order of magnitude lower than in normal vessels [28]. Therefore, the flow rate used in the current study was towards the upper limit of rates chosen to study tumour perfusing resistivity which suggests that magnetic targeting may be effective in helping retain the MBs in the tumour vasculature and allowing a greater proportion to be destroyed in an applied acoustic field.

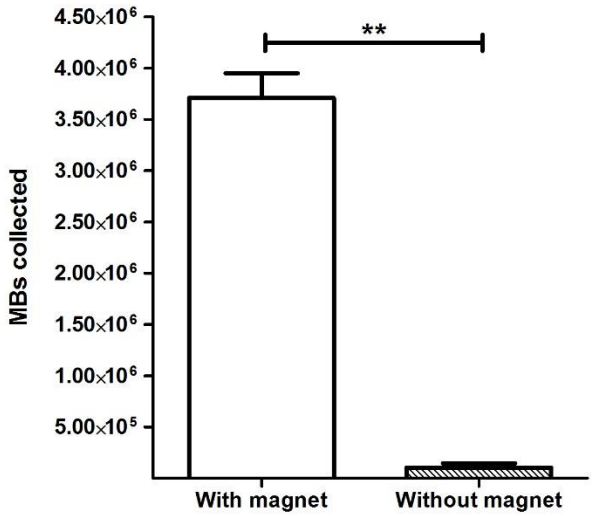

Figure 2 Plot of MBs retained after injection through a flow-cell in the presence and absence of a fixed magnet.

In order to retain a useful proportion (10%) of injected microbubbles at these blood flow rates, an estimated magnetic field gradient of 0.15 T/m would provide sufficient force to capture superparamagnetic particles flowing the capillary vessels [29]. When considering the possible translation of such technology to the clinic, both transabdominal and endoscopic sources are viable methods for the delivery of magnetic fields to the pancreas. In the context of the above capillary flow rates, optimized permanent magnet designs with a volume of 1.02 cm^3 [20] would

be capable of targeting a tumour through the duodenal wall as part of an endoscopic probe, where the approximate distance to the head of the pancreas is in the region of 10 mm. In the case of transabdominal delivery, where the distances are more variable depending on the patient's body to mass index (BMI), the optimised permanent magnet volume would be in the region of 1.66 cm^3, based on a distance of 50 mm from the outside of the abdomen to the pancreas. Even at flow rates 5 times higher than the capillary flow rate used above, the estimated field gradient to retain the same fraction of MBs would be 2.48 T/m, requiring permanent magnet volumes in the region of 1.5 cm^3 for an endoscopic device, which is readily achievable [30]. Given endoscopic ultrasound (EUS) analysis is a common diagnostic tool used in staging pancreatic cancer, a EUS device configured to deliver both magnetic and ultrasonic fields is one possibility for the translation of this technology to clinic.

In a previous study, we demonstrated the benefit of combining Rose Bengal mediated SDT and 5-FU treatment, delivered using a non-magnetic O_2MB platform, for the treatment of pancreatic cancer [6]. In the current study, we were keen to ensure that the presence of redox active Fe(II) and Fe(III) in the MB shell, would not hamper the effectiveness of SDT or 5-FU treatment. Therefore, the next step was to determine the toxicity of the combined treatment in a panel of pancreatic cancer cell lines. Human pancreatic BxPC-3, MiaPaCa-2 and Panc-01 cells were chosen as targets in addition to the T110299 cell line [31]. The latter was isolated from a primary pancreatic tumour in the KPC model (Ptf1a-Cre; LSL-$Kras^{G12D}$ and Ptf1aCre; LSL-$Kras^{G12D}$; LSL-$Trp^{53fl/R172H}$ mice, respectively, that were back-crossed on a C57BL/6 background). The cells were seeded in 96 well plates and treated with a suspension of either $MagO_2$MB-5FU, $MagO_2$MB-RB or combined $MagO_2$MB-5FU / $MagO_2$MB-RB treatment in the presence of ultrasound. Untreated cells and cells treated with ultrasound only were used as controls.

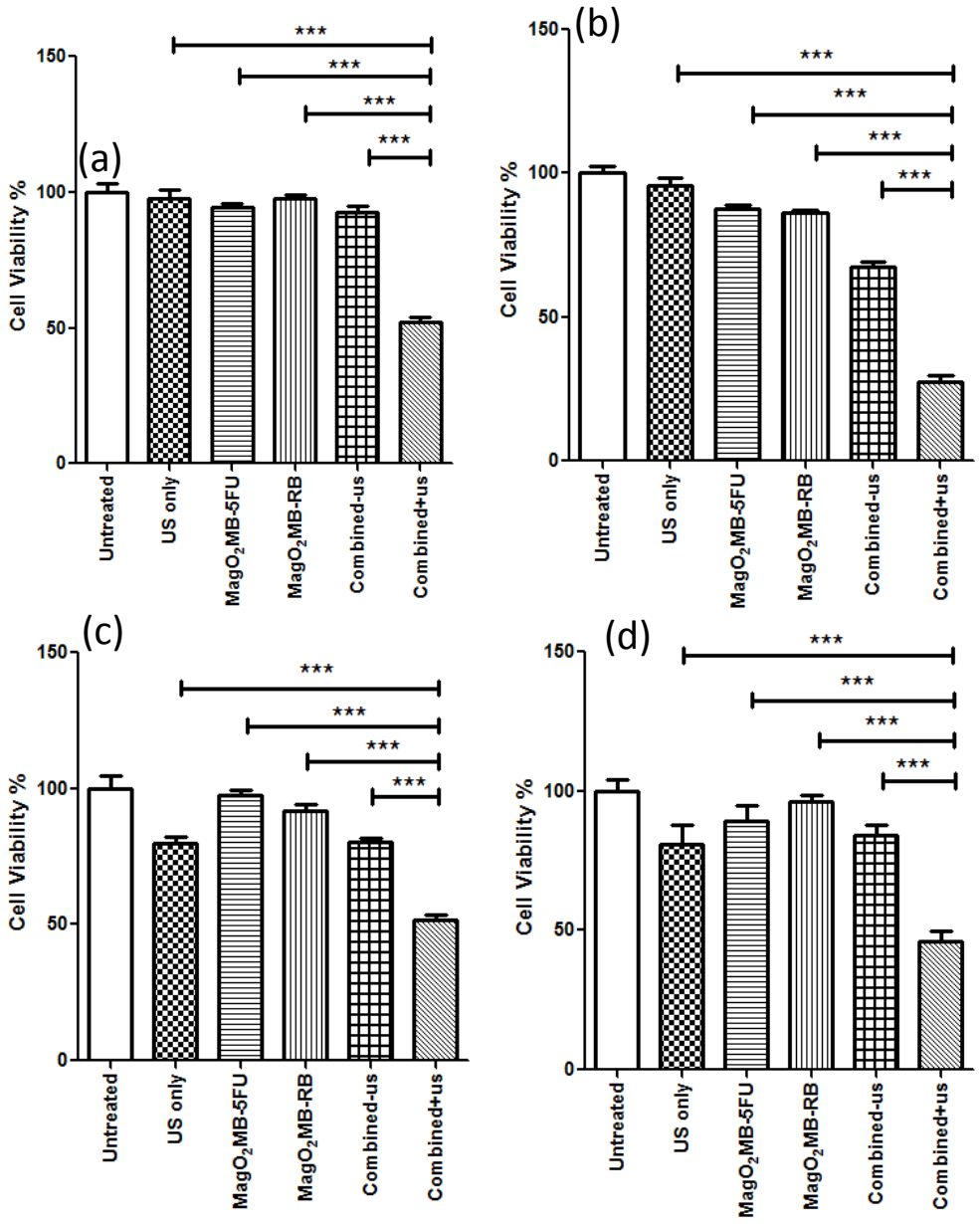

Figure 3 Plot of % cell viability for (a) BxPC-3 (b) T110299 (c) MiaPaCa-2 and (d) Panc-01 after treatment with (i) untreated, (ii) ultrasound only (iii) $MagO_2$MB-5FU only (iv) $MagO_2$MB-RB only,

(v) combined $MagO_2$MB-RB and $MagO_2$MB-5FU and (vi) combined $MagO_2$MB-RB and $MagO_2$MB-5FU plus ultrasound. *** $p < 0.001$ for (vi) compared to either (ii), (iii), (iv), or (v).

The results are shown in Figure 3 and reveal a significant reduction ($p<0.001$) in cell viability for all cell lines that received combined SDT and 5-FU treatment with reductions greater than 50% relative to the untreated cells. In contrast, both the $MagO_2$MB-5FU and $MagO_2$MB-RB formulations demonstrated only minor reductions (< 10%) in the absence of ultrasound treatment meaning it was possible to control the generation of cytotoxicity using the ultrasound stimulus. Therefore, these results suggest that application of ultrasound not only disrupts the MBs releasing the encapsulated O_2 gas and the attached Rose Bengal / 5-FU into the extracellular medium but also activates Rose Bengal leading to ROS generation and the observed cytotoxic effect [32] It is also possible that application of the ultrasound could be enhancing the action of 5-FU by means of sonoporation.. Indeed, it has been shown that this strategy can be employed to enhance the action of cancer chemotherapeutics by affording transient intracellular access of the drug via sonoporation [33].

While the *in vitro* cytotoxicity of the combined 5-FU / SDT treatment was encouraging, *in vivo* experiments are essential to identify the benefit of magnetic targeting. To this end, orthotopic human xenograft BxPC-3-Luc pancreatic tumours were established in SCID mice. Nineteen days following implantation the mice were randomly distributed into three groups (n=4). Group 1 received no treatment; Group 2 received a $MagO_2$MB-5FU / $MagO_2$MB-RB suspension administered intravenously with the tumour region exposed to low-intensity ultrasound during and following injection for a total exposure of 3.5 min. Group 3 also received an IV injection of the $MagO_2$MB-5FU / $MagO_2$MB-RB suspension but in addition to ultrasound treatment, a permanent magnet was also directed at the tumour during ultrasound treatment (3.5 min). Treatments were repeated on days 20 and 21 with the mice sacrificed on day 28 [34]. This treatment schedule was determined on the basis of a previous pilot study where multiple

treatments in close succession were shown to be beneficial over a single treatment. In addition, as our primary goal is to use this technology as a neo-adjuvant treatment to downstage tumours in advance of surgery, aggressive treatment of the tumours with three successive administrations was the preferred choice and as the technology is targeted, significantly lower concentrations of RB and 5-FU are used compared to standard systemic administration. Once the mice were sacrificed, the tumours were surgically excised and volumes determined with the results for the three groups shown in Figure 4.

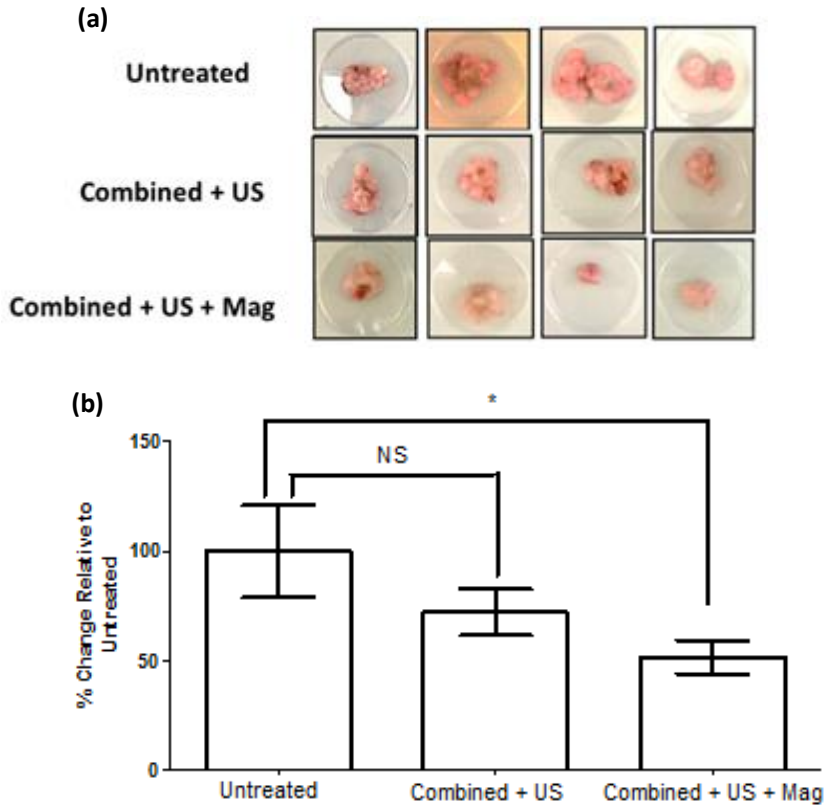

Figure 4 (a) Photographs of orthotopic BxPC-3 Luc tumours removed from SCID mice 28 days following implantation after (i) no treatment (top), (ii) treatment with combined $MagO_2MB$-RB and $MagO_2MB$-FU plus ultrasound (middle) or (iii) treatment with $MagO_2MB$-RB and $MagO_2MB$-FU plus ultrasound and magnet (bottom). Treatments were administered on day(s) 19, 20 and 21. (b) Plot of % change in tumour volume relative to untreated for mice treated with (ii) or (iii)

above. * p < 0.05 for (iii) compared to (i). A one-way ANOVA, post-Hoc test showed the same significance as above.

A statistically significant reduction in tumour volume of 48.3% ($p<0.05$) was observed for Group 3 relative to control Group 1, while for Group 2 an obvious downward trend in tumour volume (27.9%) was detected although this was not found to be statistically significant. This improvement in efficacy in the presence of a magnetic field could be due to more MBs being retained in the tumour microenvironment, so that ultrasound exposure can enable enhanced deposition of MB payloads and subsequent activation of the sensitiser. Although the latter would require verification by further experimentation, our suggestion is corroborated by the observation that, activated caspase and BAX protein levels were both significantly elevated in tumours harvested from Group 3, when compared to expression of those proteins in tumours from either of the other 2 groups ($p<0.05$) (Figure 5).

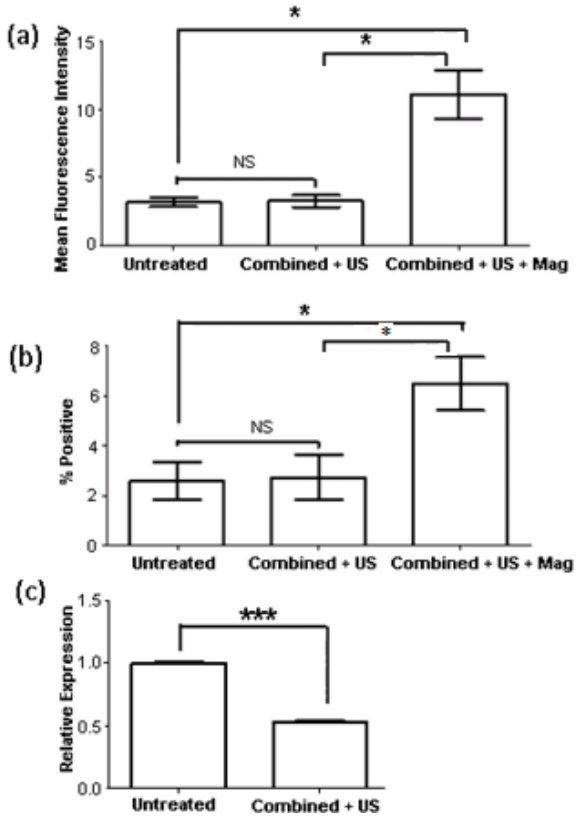

Figure 5 (a) Plot showing presence of active caspase in single cell suspensions of tumours removed from SCID mice 38 days following implantation after treatment with (i) no treatment (left), (ii) treatment with combined $MagO_2MB$-RB and $MagO_2MB$-5FU plus ultrasound (middle) or (iii) treatment with $MagO_2MB$-RB and $MagO_2MB$-5FU plus ultrasound and magnet (right). Fluorescence indicates caspase activity which is reflective of apoptosis and was determined using the Pan Caspase probe (Pan Caspase NIR from Vergent Bioscience) via flow cytometry. Treatments were administered on Days 19, 20 and 21. (b) BAX protein expression of the same single cell suspensions via flow cytometry. *$p < 0.05$ for (iii) compared to (i). (c) Relative expression of TMBIM1 in untreated control tumours and those receiving combined treatment. ***$p<0.001$.

Increases in activated caspase and BAX protein levels are indicative of increased apoptosis and consistent with the increased treatment efficacy observed for Group 3. Although BAX and caspase were not significantly increased in group 2, a trend in tumour size reduction was observed for this group (Figure 4). In addition, previous studies have shown that ectopic BxPC-3 tumours receiving the combined treatment in the absence of a magnetic field resulted in decreased tumour size and expressed markers for increased apoptosis [6]. Although significant differences exist in the manner in which this and the previous study were performed both from the perspective of the model type (orthotopic vs. ectopic) and that of the dosing regimen (multiple vs. single), it was felt that the reduction 'trend' observed in group 2 in the current study (Fig.4) warranted further consideration. To this end, we have been able to use qRT-PCR analysis to demonstrate that TMBIM1 (encoding transmembrane BAX inhibitor motif containing 1) was significantly downregulated in tumours receiving the combined treatment in the absence of a magnetic field (Figure 5). Since TMBIM1 is an inhibitor of BAX [35], its down regulation in these tumours could lead to enhanced BAX-mediated apoptosis without an observable change in BAX concentration. However, the authors do realise that the data presented in figures 4 and 5 were derived from tumours removed at a specific time point (9 days) following treatment and these data may differ if longer or shorter time-points were chosen. Continuing studies will include a more in-depth examination of gene expression at various time points in order to more

clearly elucidate the interplay between both of these genes and their role in treatment-induced apoptosis.

It was also found during the above studies that animals receiving the magnetically-responsive platform did not suffer any overt adverse effects and no significant change in body weight was observed over the course of the experiment (Figure 6a). To investigate the aspect of safety further, a more detailed toxicology study was undertaken. This involved administering the $MagO_2$MB-5FU / $MagO_2$MB-RB suspension to 10 healthy non-tumour bearing MF1 mice by tail vein injection on Days 0 and 8. Similar experiments were undertaken involving MF1 mice treated with 5-FU or Rose Bengal alone at concentrations higher than those present on the MagMBs to reflect clinical doses, while untreated animals served as a control group. Blood samples were harvested from each group of animals on Day 15 and analysed for a range of key biochemical markers (Figure 6b). No major differences in profile were observed between the $MagO_2$MB-5FU / $MagO_2$MB-RB group and the other groups that would raise any concern regarding toxicity of the combined MB-based treatment. Indeed ALT activity, which is a measure of liver function, was lower in the $MagO_2$MB-5FU / $MagO_2$MB-RB group compared to the other groups. While there was an increase in platelet and lymphocyte levels for the $MagO_2$MB-5FU / $MagO_2$MB-RB group relative to the untreated group, levels were also raised in 5-FU and Rose Bengal treated animals and the differences between these groups were not significant.

(a)

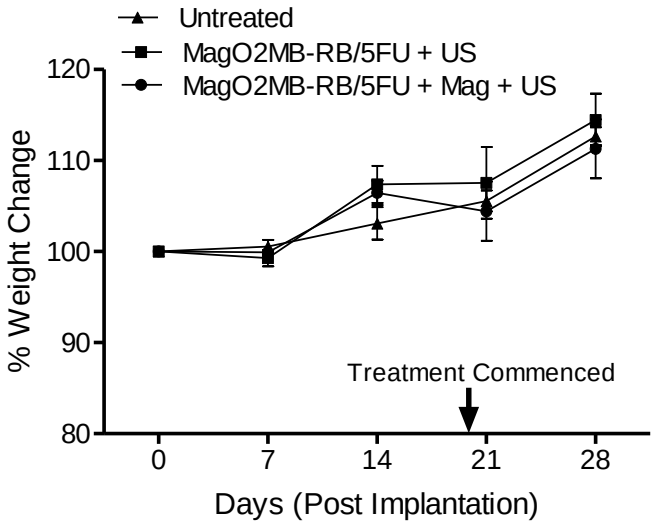

(b)

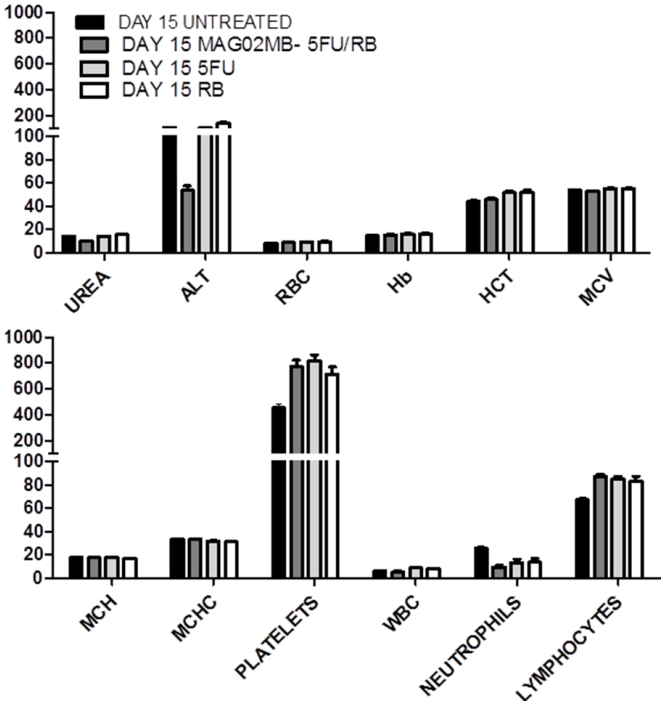

Figure 6 (a) Average body weight of mice recorded following treatment with vehicle only (triangles), a suspension of $MagO_2$MB-RB / MagO2MB-5FU + ultrasound (squares), or a suspension of $MagO_2$MB-RB / $MagO_2$MB-5FU + ultrasound + magnet (circles). (b) Whole blood and serum biochemistry analysis from healthy MF1 mice (i) untreated control, or treated with (ii) a suspension of $MagO_2$MB-RB / $MagO_2$MB-5FU, (iii) 5-FU alone, or (iv) RB alone.

Similarly, there was evidence of mild neutropenia in the three treatment groups relative to the untreated group, but again the difference between the $MagO_2$MB-5FU / $MagO_2$MB-RB group and the 5-FU and RB groups was not significant. Furthermore, histological analysis of liver and kidney sections removed post-mortem on Day 16 also revealed no significant changes between the $MagO_2$MB-5FU / $MagO_2$MB-RB group and the 5-FU or RB treated groups (Figure 7).

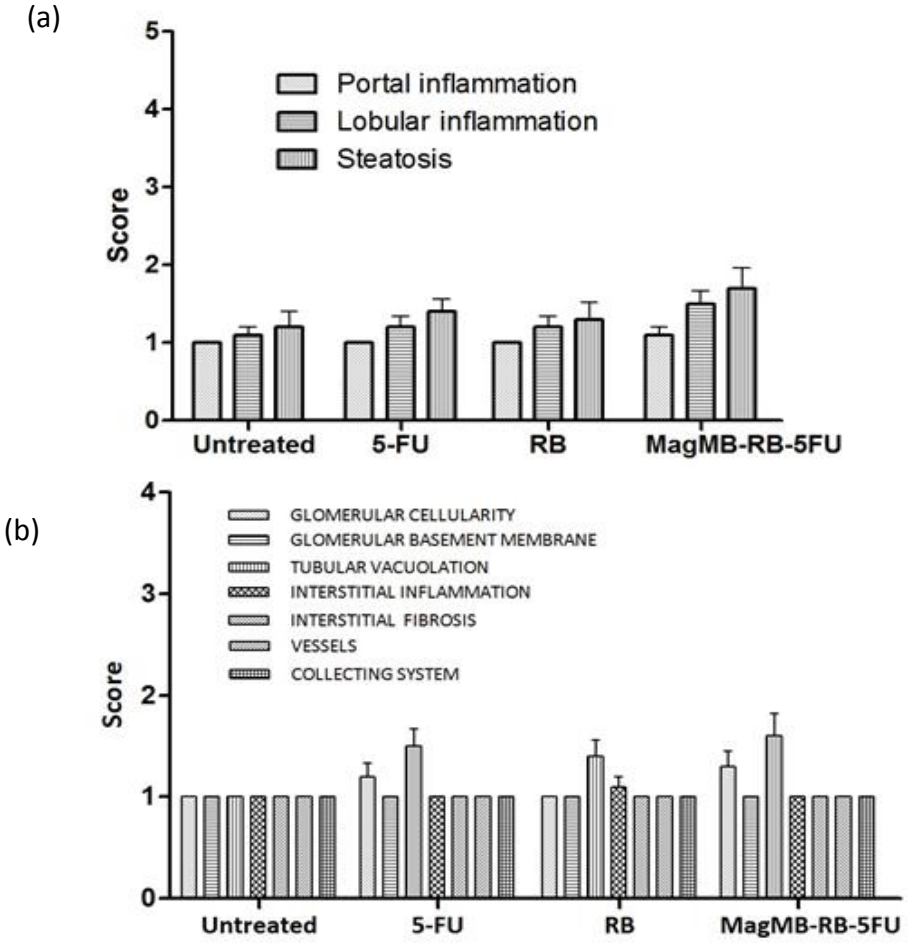

Figure 7 Scoring for sections of (a) liver and (b) kidney following (i) no treatment, or treatment with (ii) 5-FU alone, (iii) RB alone, or (iv) a suspension of $MagO_2$MB-RB / $MagO_2$MB-5FU conjugates. Portal inflammation scored 1-5 while all other parameters were scored from 1-4. In each case a score of 1 = normal.

There was evidence of a slight increase in liver steatosis score for the $MagO_2$MB-5FU / $MagO_2$MB-RB group but this was not significant when compared to the 5-FU or RB groups. Liver steatosis, also known as fatty liver disease, is normally a consequence of dietary or lifestyle habits but can also be influenced by certain chemotherapeutic drugs including antimetabolites [36]. The slight increase in score for the $MagO_2$MB-5FU / $MagO_2$MB-RB group relative to 5-FU or RB may be due to the uptake and metabolism of the lipid component of the MBs and on that basis is likely a transient change of limited clinical significance. Analysis of kidney sections showed slightly raised levels of glomerular cellularity and tubular vacuolation for the $MagO_2$MB-5FU / $MagO_2$MB-RB group, but again these levels were also raised in the 5-FU and RB groups and the differences were non-significant. Some of the tubular vacuolation may have been artefactual, possibly fixation related, as it was observed in both treated and untreated groups. It must be stressed, however, that any effect observed in the liver or kidney histology analysis was deemed to be mild and in no case did the mean score exceed 2. Collectively, these results indicate the potential of O_2MagMBs as a safe and effective platform for the delivery of combined antimetabolite and SDT treatment of pancreatic cancer.

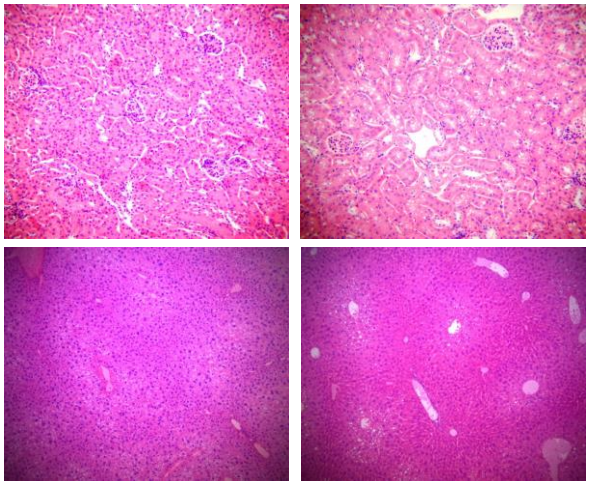

Figure 8 Representative H&E stained microscope images of liver (top) and kidney (bottom) sections taken from animals sacrificed on day 15 following treatment with a suspension of $MagO_2$MB-RB / $MagO_2$MB-5FU (right) or untreated (left).

4.0 Conclusions: Magnetically responsive MBs were successfully prepared and shown to be retained at a target site in the presence of an externally applied magnetic field. When decorated with the sensitiser Rose Bengal and the antimetabolite 5-FU, the $MagO_2MB$ conjugates produced reductions of greater than 50% in the viability of four pancreatic cancer cell lines upon exposure to relatively low intensity ultrasound. The combined application of external magnetic and ultrasound fields during IV delivery of the $MagO_2MB$ conjugates resulted in a 48.3% reduction in orthotopic pancreatic tumour volumes 9 days after treatment relative to the control group, while the application of ultrasound alone resulted in a reduction of only 27.9%. In addition, a significant increase in apoptosis was observed in tumours that were treated with the MagMB conjugates and exposed to both magnetic and ultrasonic fields when compared to the ultrasound alone or untreated groups. These results highlight the potential of using a combination of magnetic and ultrasonic fields to retain and disrupt MBs in the tumour vasculature. The results also confirm the effectiveness of combined sonodynamic / antimetabolite therapy delivered using the $MagO_2MB$ platform as a safe, highly targeted and efficacious treatment for pancreatic cancer.

5.0 Acknowledgements: JFC thanks Norbrook Laboratories Ltd for an endowed chair. ES and JO thank the Engineering and Physical Sciences Research Council for support through grant EP/I021795/1. EB thanks the Research Councils UK Digital Economy Programme for support through grant EP/G036861/1 (Oxford Centre for Doctoral Training in Healthcare Innovation). We also thank Prof. Jens Siveke at Medizinische Klinik; Klinikum rechts der Isar; Technische Universität München ; Munich, Germany for the KPC cell line. We acknowledge Dangoor Education for their supporting RH in this work.

6.0 References:

[1] S. Badger, J. Brant, C. Jones, J. McClements, M. Loughrey, M. Taylor, T. Diamond, L. McKie, The role of surgery for pancreatic cancer: a 12-year review of patient outcome, Ulster Med. J. 79 (2010) 70-75.

[2] J. Li, M.G. Wientjes, J.L. Au, Pancreatic cancer: pathobiology, treatment options, and drug delivery, The AAPS journal. 12 (2010) 223-232.

[3] M.H. Katz, P.W. Pisters, D.B. Evans, C.C. Sun, J.E. Lee, J.B. Fleming, J.N. Vauthey, E.K. Abdalla, C.H. Crane, R.A. Wolff, Borderline resectable pancreatic cancer: the importance of this emerging stage of disease, J. Am. Coll. Surg. 206 (2008) 833-846.

[4] M. Tachezy, F. Gebauer, C. Petersen, D. Arnold, M. Trepel, K. Wegscheider, P. Schafhausen, M. Bockhorn, J.R. Izbicki, E. Yekebas, Sequential neoadjuvant chemoradiotherapy (CRT) followed by curative surgery vs. primary surgery alone for resectable, non-metastasized pancreatic adenocarcinoma: NEOPA-a randomized multicenter phase III study (NCT01900327, DRKS00003893, ISRCTN82191749), BMC Cancer. 14 (2014) 1.

[5] C. Hamill. SBRT pre-operatively for borderline resectable pancreatic cancer. In: UK Clinical Trials Gateway website. Study ID Numbers:OCTO_054 (2014).

[6] C. McEwan, S. Kamila, J. Owen, H. Nesbitt, B. Callan, M. Borden, N. Nomikou, R.A. Hamoudi, M.A. Taylor, E. Stride, Combined sonodynamic and antimetabolite therapy for the improved treatment of pancreatic cancer using oxygen loaded microbubbles as a delivery vehicle, Biomaterials. 80 (2016) 20-32.

[7] S. Sirsi, M. Borden, Microbubble compositions, properties and biomedical applications, Bubble Science, Engineering & Technology. 1 (2009) 3-17.

[8] V. Stewart, P. Sidhu, New directions in ultrasound: microbubble contrast, Br. J. Radiol. (2014).

[9] G. Dimcevski, S. Kotopoulis, T. Bjånes, D. Hoem, J. Schjøtt, B.T. Gjertsen, M. Biermann, A. Molven, H. Sorbye, E. McCormack, A human clinical trial using ultrasound and microbubbles to enhance gemcitabine treatment of inoperable pancreatic cancer, J. Controlled Release. 243 (2016) 172-181.

[10] S. Kotopoulis, G. Dimcevski, O. Helge Gilja, D. Hoem, M. Postema, Treatment of human pancreatic cancer using combined ultrasound, microbubbles, and gemcitabine: a clinical case study, Med. Phys. 40 (2013).

[11] S. Umemura, N. Yumita, R. Nishigaki, K. Umemura, Mechanism of cell damage by ultrasound in combination with hematoporphyrin, Jap. J. Cancer Res. 81 (1990) 962-966.

[12] H. Chen, J.H. Hwang, Ultrasound-targeted microbubble destruction for chemotherapeutic drug delivery to solid tumors, Journal of therapeutic ultrasound. 1 (2013) 1.

[13] S. Hernot, A.L. Klibanov, Microbubbles in ultrasound-triggered drug and gene delivery, Adv. Drug Deliv. Rev. 60 (2008) 1153-1166.

[14] M.M.A. Valenzuela, J.W. Neidigh, N.R. Wall, Antimetabolite treatment for pancreatic cancer, Chemotherapy. 3 (2014).

[15] D. Costley, C. Mc Ewan, C. Fowley, A.P. McHale, J. Atchison, N. Nomikou, J.F. Callan, Treating cancer with sonodynamic therapy: a review, International Journal of Hyperthermia. 31 (2015) 107-117.

[16] N. Nomikou, C. Fowley, N.M. Byrne, B. McCaughan, A.P. McHale, J.F. Callan, Microbubble–sonosensitiser conjugates as therapeutics in sonodynamic therapy, Chemical Communications. 48 (2012) 8332-8334.

[17] C. McEwan, J. Owen, E. Stride, C. Fowley, H. Nesbitt, D. Cochrane, C.C. Coussios, M. Borden, N. Nomikou, A.P. McHale, Oxygen carrying microbubbles for enhanced sonodynamic therapy of hypoxic tumours, J. Controlled Release. 203 (2015) 51-56.

[18] Y. Gao, C.U. Chan, Q. Gu, X. Lin, W. Zhang, D.C.L. Yeo, A.M. Alsema, M. Arora, M.S.K. Chong, P. Shi, Controlled nanoparticle release from stable magnetic microbubble oscillations, NPG Asia Materials. 8 (2016) e260.

[19] J. Owen, P. Rademeyer, D. Chung, Q. Cheng, D. Holroyd, C. Coussios, P. Friend, Q.A. Pankhurst, E. Stride, Magnetic targeting of microbubbles against physiologically relevant flow conditions, Interface focus. 5 (2015) 20150001.

[20] C. Crake, J. Owen, S. Smart, C. Coviello, C. Coussios, R. Carlisle, E. Stride, Enhancement and Passive Acoustic Mapping of Cavitation from Fluorescently Tagged Magnetic Resonance-Visible Magnetic Microbubbles In Vivo, Ultrasound Med. Biol. 42 (2016) 3022-3036.

[21] J. Ciccolini, C. Mercier, M. Blachon, R. Favre, A. Durand, B. Lacarelle, A simple and rapid high-performance liquid chromatographic (HPLC) method for 5-fluorouracil (5-FU) assay in plasma and possible detection of patients with impaired dihydropyrimidine dehydrogenase (DPD) activity, J. Clin. Pharm. Ther. 29 (2004) 307-315.

[22] L.C. Barnsley, D. Carugo, J. Owen, E. Stride, Halbach arrays consisting of cubic elements optimised for high field gradients in magnetic drug targeting applications, Phys. Med. Biol. 60 (2015) 8303.

[23] A. McHale, L. McHale, Use of a tetrazolium based colorimetric assay in assessing photoradiation therapy in vitro, Cancer Lett. 41 (1988) 315-321.

[24] L.C. Barnsley, D. Carugo, E. Stride, Optimized shapes of magnetic arrays for drug targeting applications, J. Phys. D. 49 (2016) 225501.

[25] K. Ishak, A. Baptista, L. Bianchi, F. Callea, J. De Groote, F. Gudat, H. Denk, V. Desmet, G. Korb, R.N. MacSween, Histological grading and staging of chronic hepatitis, J. Hepatol. 22 (1995) 696-699.

[26] D.E. Kleiner, E.M. Brunt, M. Van Natta, C. Behling, M.J. Contos, O.W. Cummings, L.D. Ferrell, Y. Liu, M.S. Torbenson, A. Unalp-Arida, Design and validation of a histological scoring system for nonalcoholic fatty liver disease, Hepatology. 41 (2005) 1313-1321.

[27] E.N. Marieb, K. Hoehn, The cardiovascular system: blood vessels, Human anatomy & physiology. (2013) 703-720.

[28] R.K. Jain, T. Stylianopoulos, Delivering nanomedicine to solid tumors, Nature reviews Clinical oncology. 7 (2010) 653-664.

[29] L.C. Barnsley, D. Carugo, M. Aron, E. Stride, Understanding the dynamics of superparamagnetic particles under the influence of high field gradient arrays, Phys. Med. Biol. 62 (2017) 2333.

[30] T. Krings, J. Finney, P. Niggemann, P. Reinacher, N. Lück, A. Drexler, J. Lovell, A. Meyer, R. Sehra, P. Schauerte, Magnetic versus manual guidewire manipulation in neuroradiology: in vitro results, Neuroradiology. 48 (2006) 394-401.

[31] P. Duewell, E. Beller, S.V. Kirchleitner, T. Adunka, H. Bourhis, J. Siveke, D. Mayr, S. Kobold, S. Endres, M. Schnurr, Targeted activation of melanoma differentiation-associated protein 5 (MDA5) for immunotherapy of pancreatic carcinoma, Oncoimmunology. 4 (2015) e1029698.

[32] We have previously demonstrated in Ref 6 the effects of combined RB and 5-FU treatment (5 μM and 100 μM respectively) as free agents (i.e. not as MB conjugates) to cause between 20-30% reduction in viability in BxPC-3, MiaPaCa-2 and Panc-01 cell lines.

[33] N. Nomikou, A.P. McHale, Exploiting ultrasound-mediated effects in delivering targeted, site-specific cancer therapy, Cancer Lett. 296 (2010) 133-143.

[34] The treatment schedule and termination date was informed by an earlier pilot study and supported by bioluminescent imaging.

[35] D.A. Lisak, T. Schacht, V. Enders, J. Habicht, S. Kiviluoto, J. Schneider, N. Henke, G. Bultynck, A. Methner, The transmembrane Bax inhibitor motif (TMBIM) containing protein

family: Tissue expression, intracellular localization and effects on the ER CA 2 -filling state, Biochimica et Biophysica Acta (BBA)-Molecular Cell Research. 1853 (2015) 2104-2114.

[36] K. Miyake, K. Hayakawa, M. Nishino, T. Morimoto, S. Mukaihara, Effects of Oral 5-Fluorouracil Drugs on Hepatic Fat Content in Patients With Colon Cancer 1, Acad. Radiol. 12 (2005) 722-727.